Anisotropy of laser emission in monoclinic Nd:$ScYSiO_5$ crystals cut along the optical indicatrix axes

Shande Liu (刘善德)[1,*], Lihe Zheng (郑丽和)[2], Jun Xu (徐 军)[2], Yuping Zhang (张玉萍)[1], Huiyun Zhang (张会云)[1], Dehua Li (李德华)[1], Tingqi Ren (任廷琦)[1,], Baitao Zhang (张百涛)[3], and Jingliang He (何京良)[3]**

[1]*College of Electronic, Communication and Physics, Shandong University of Science and Technology, Qingdao 266590, China*

[2]*Shanghai Institute of Ceramics, Chinese Academy of Science, Shanghai 200050, China*

[3]*State Key Laboratory of Crystal Materials, Shandong University, Ji'nan 250100, China*

**Corresponding author: pepsl_liu@163.com; **corresponding author: rentingqi@126.com*

Received November 2, 2015; accepted December 11, 2015; posted online January 27, 2016

In this Letter, we demonstrate the anisotropy of laser emission in disordered Nd:$ScYSiO_5$ (Nd:SYSO) crystals cut along the optical indicatrix axes. High-powered lasers with different oscillation wavelengths and polarizations are realized by using different oriented crystals as gain media. For Y-cut crystals, the dual-wavelength laser vibration direction is found to be along the X axis and a maximum output power of 9.43 W is obtained, giving an optical-to-optical conversion efficiency of 48.8% and a slope efficiency of 51.3%. For X- and Z-cut crystals, 1075 and 1078 nm lasers operating orthogonally polarize oscillate with total output powers of 7.07 and 8.43 W, respectively. The experimental results reveal that the intrinsic anisotropy for the monoclinic disordered laser crystals could make laser design flexible and controllable.

OCIS codes: 140.3380, 140.3540.

doi: 10.3788/COL201614.021406.

Diode-pumped solid-state lasers can find wide applications in many fields such as military, scientific research, laser microsurgery, and optical communication[1–3]. Because of the gain competition, only one wavelength (or line) can normally be obtained from the laser systems, despite several laser transitions being present in the laser crystals. Recently, the development of laser radar, spectral analysis, and THz technology accelerated the research of simultaneous dual-wavelength lasers[4–6]. Nd:YVO_4, Nd:$GdVO_4$, and Nd:$LuVO_4$ lasers have been demonstrated to achieve simultaneous dual-wavelength laser emissions in which an additional birefringent element or second laser crystal was employed[7–10]. Many disordered crystals are also used as multiwavelength laser materials such as Nd:CNGG[11], Nd:GYSGG[12], Tm:LuAG[13], Yb:KLW[14], Yb-Tm:KLW[15], Nd:LYSO[16], and Tm:LYSO[17]. Multiple types of the substitutional sites in this crystal provide a strong inhomogeneous lattice field for rare earth ions, which results in large ground-state splitting and broad emission spectra. Therefore, it is helpful to obtain multiwavelength and ultrafast laser operations.

Among these disordered crystals, monoclinic silicate crystals have attracted a lot in the dual-wavelength laser research area due to several advantaged factors. One factor is that anisotropy of the crystal structure in the monoclinic crystal leads to anisotropy of the laser characteristics. The other is that the silicate crystals possess good crystal growth habits and excellent physical and chemical properties. A novel crystal, Nd:$ScYSiO_5$ (Nd:SYSO), was grown by the Shanghai Institute of Ceramics with the Czochralski method along the crystallographic b axis. The presence of multitype sites in the crystal provides a strong inhomogeneous lattice field, which leads to a large ground-state split and broadened emission spectra. Hence, the multiwavelength operation in a cw and Q-switched Nd:SYSO laser was reported[18]. The passively mode-locking of Nd:SYSO crystal was realized with a semiconductor saturable absorber mirror (SESAM)[19]. Of all the previous results, the optical propagation direction along the crystallographic b axis and the total output power is just on the watt class level.

Here, the anisotropy of laser operations along different orientations of the Nd:SYSO crystals was demonstrated and well explained by the fluorescence emission spectra. For X- and Z-cut crystals, 7.07 and 8.43 W dual-wavelength laser operations both at 1075 and 1078 nm were obtained, respectively. The polarization states were both found to be orthogonally polarized. With Y-cut crystals, the laser polarization state was along the X axis and a maximum dual-wavelength output power of 9.43 W was achieved at an absorbed pump power of 19.32 W, corresponding to an optical-to-optical conversion efficiency of 48.8%.

A compact concave-plano cavity was employed, as shown in Fig. 1. The pump source was a fiber-coupled laser diode (LIMO70-F200-DL808-FP-A) emitting at 808 nm with a radius of 200 μm and a numerical aperture (NA) of 0.22. The pump beam was coupled into the laser crystals with a coupling system and the waist radius was about 200 μm. The laser cavity was made up of an input mirror M_1, a Nd:SYSO crystal, and an end mirror M_2. The overall cavity length was 15 mm. M_1 was a plano-concave mirror

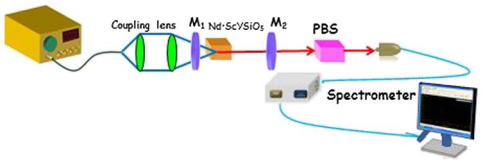

Fig. 1. Schematic arrangement of the experimental laser setup.

with a curvature radius of 250 mm. The plane was anti-reflection coated at 808 nm (AR, $R < 0.2\%$); the concave face was coated for high transmission at 808 nm (HT, $T > 95\%$) and high-reflection (HR, $R > 99.8\%$) coated at 1000–1110 nm. The output coupler M_2 was coated with partial transmission ($T_{oc} = 5\%$, 10%, and 40% were available) at 1060–1080 nm. The Nd:SYSO crystals cut along the X, Y, and Z optical indicatrix axes were used as the laser medium. All crystal samples were processed in dimension of $3 \times 3 \times 8$ (mm), and both of the end faces were uncoated. The crystals were wrapped with indium foil and mounted in a copper block cooled by water at a temperature of 20°C. A polarization-dependent beam splitter (Thorlabs, CM1-PBS25-1064-HP) was used to measure the polarization direction of the Nd:SYSO lasers. The average output power was measured by a power meter (Coherent, Field-Max II), and the laser spectra were recorded by an optical analyzer (0.5 nm spectral resolutions, Avantes, AcaSpec-3648-NIR256-2.2).

As a biaxial crystal, the Nd:SYSO have three optical indicatrix axes with different refractive indexes. In its monoclinic structure, one of the optical indicatrix axes is collinear with the two-fold axis of the crystal, i.e., the crystallographic axis b. The other two optical indicatrix axes lie in the (0,1,0) face (perpendicular to the crystallographic axis b) at a specific angle with the crystallographic axes a and c. The angles between the crystallographic axes are $\beta_{ab} = 90°, \beta_{bc} = 90°$, and $\beta_{ac} = 102.7°$. A b-cut Nd:SYSO crystal sample (1 mm thick) is used to measure, with an XPT-6-type polarizing microscope, and the results have shown in Fig. 2. The angle between one of the optical indicatrix axis and the a axis is measured to be 24.5°, and the angle between the other optical indicatrix axis and the c axis is 11.8°. The definition of X, Y, and Z optical indicatrix axes follows the principle of $n_X < n_Y < n_Z$.

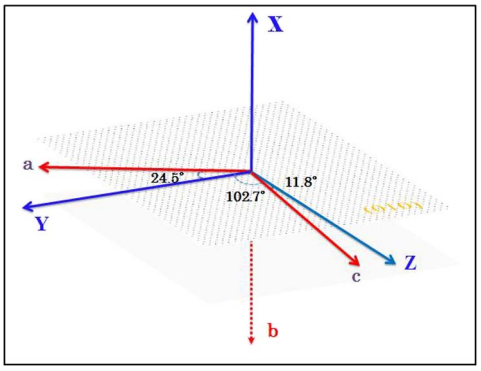

Fig. 2. Relationships between the principal axes (X, Y, Z) and the crystallographic axes (a, b, c): $\beta_{aY} = 24.5°$ and $\beta_{cZ} = 11.8°$.

With 0.8 at.% Nd^{3+}-doped SYSO crystals, we processed X-, Y-, and Z-cut samples. The dimensions of the crystals are $3 \times 3 \times 10$ (mm) (3 and 10 mm directions are all principle axes) and 10 mm is the transmission direction. With a JASCO V570 model UV/VIS/NIR spectrophotometer, the absorption spectra were recorded at room temperature. As shown in Fig. 3, the absorption peak value around 800 nm for all the crystal samples is located at 809 nm, and intensities are 0.698, 0.935, and 0.812 for X-cut, Y-cut, and Z-cut, respectively.

Using the same crystal samples, we measured the polarized fluorescence spectra by an Edinburgh FS920 High Sensitive Fluorescence Spectrometer (<0.09 nm resolution, 1200 g/mm grating). The simulated emission cross section was calculated with the formula expressed as

$$\sigma_{\mathrm{em}}(\lambda) = \frac{\lambda^4 I(\lambda)}{8\pi c n^2 \tau_{\mathrm{rad}} \int I(\lambda)\mathrm{d}\lambda}.$$

The polarized emission cross-section spectra are shown in Fig. 4, and the peak information for ${}^4\mathrm{F}_{3/2} \rightarrow {}^4\mathrm{I}_{11/2}$ transitions around 1.08 μm are also listed in Table 1; the maximum emission peak both are located at 1077.3 nm for X and Z polarization, while located at 1074.2 nm for Y polarization. The different peak emission wavelengths at different polarizations of the crystals suggest the potentiality that different laser wavelengths may be realized by using different oriented crystals as gain media.

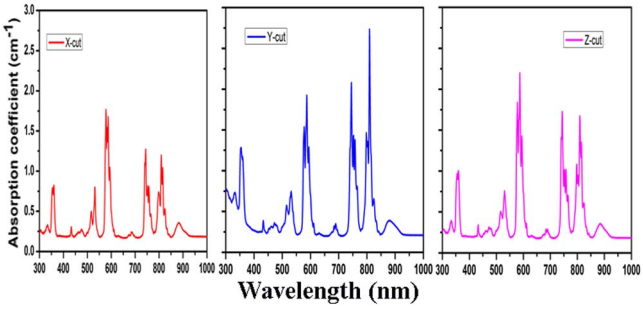

Fig. 3. Room temperature absorption spectra for the X-, Y-, and Z-cut Nd:SYSO crystals.

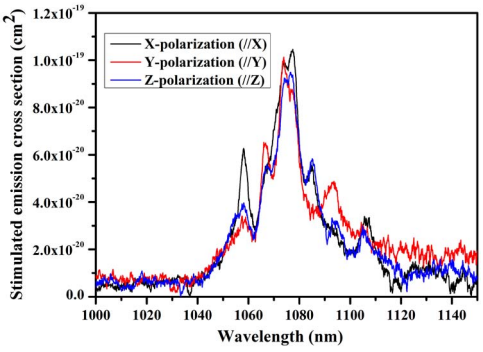

Fig. 4. Polarized emission cross-section spectra for the X-, Y-, and Z-cut Nd:SYSO crystals.

Table 1. Polarized Emission Cross Section for ${}^4F_{3/2} \rightarrow {}^4I_{11/2}$ Transition Around 1.08 μm

Peak Wavelength (nm)	X Polarization (10^{-20} cm^2)	Y Polarization (10^{-20} cm^2)	Z Polarization (10^{-20} cm^2)
1074.2	9.98	10.00	9.25
1077.3	10.46	8.76	9.37

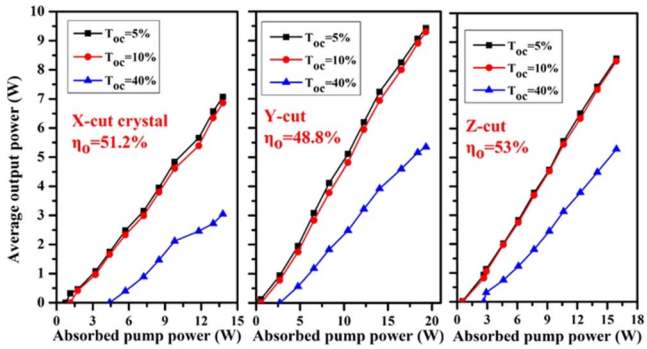

Fig. 5. Average output power with respect to the absorbed pump power.

We analyzed the dual-wavelength laser operation with the Nd:SYSO crystal in the range of 1070–1080 nm. As shown in Table 1, the Nd:SYSO crystal had the comparable emission cross sections in X, Y, and Z polarizations that were, respectively, near 1074.2 and 1077.3 nm. The threshold condition for each wavelength in dual-wavelength laser operation is given by[20]

$$P_{\mathrm{th},i} = \frac{\ln\left(\frac{1}{R_i}\right) + L_i}{2l\eta_i} \frac{h\nu_p}{\sigma_i \tau_i} \frac{1}{\iiint s_i(r,z) r_p(r,z) \mathrm{d}v}, \qquad i = 1, 2,$$

where R_i is the reflectivity, L_i is the cavity round-trip loss, l is the length of the gain medium, η_i is the quantum efficiency, and σ_i and τ_i are the stimulated emission cross section and the fluorescence lifetime at the upper level for the corresponding transition wavelength, respectively. Parameters of $h\nu_p$, $s_i(r,z)$, and $r_p(r,z)$ are, respectively, the pump photo energy, the normalized cavity mode intensity distribution, and the normalized pump intensity distribution in the laser cavity. Here, we suppose that the experimental conditions and the resonator loss are the same for all of the samples. Therefore, the stimulated emission cross section σ_i was the key factor for the pump threshold power in the laser experiment. The lasing had a larger stimulated emission cross section that will oscillate prior to the smaller one, while at high pump levels, the dual-wavelength laser might operate simultaneously. In the experiment, the laser wavelengths were located at 1075 and 1078 nm, respectively, which shifted to red with the fluorescence spectrum. Figure 5 shows the relationship between the dual-wavelength average output power and the absorbed pump power, and the main dates are also listed in Table 2. As shown in Table 2, the pump threshold power for Y-cut (with sides parallel to the X and Z axis, respectively) crystal was nearly the same as that for the Z-cut (with sides parallel to the X and Y axis, respectively) crystal. The reason was that, whether the Y-cut or the Z-cut crystal, the prior oscillation laser wavelength was 1078 nm (X polarization) with the same stimulated emission cross-section value. For the X-cut (with sides parallel to the Y and Z axis, respectively) crystal, the maximum stimulated emission cross section of 10×10^{-20} cm^2 (1075 nm, Y polarization) was less than that of the Y-cut and the Z-cut crystal. Therefore, the pump threshold power of the X-cut crystal was higher than that of the Y-cut and the Z-cut crystals.

During the laser experiment, incident LD pump powers were all increased from 0 to 30.3 W, but the maximum absorbed pump powers were 13.8, 19.3, and 15.9 W for the X-, Y-, and Z-cut crystals, respectively. For the X-cut crystal, the maximum dual-wavelength average output power was 7.07 W, giving a slope efficiency of 53.6%. Under the absorbed pump power of 9.8 W, we

Table 2. Laser Performance of Nd:SYSO Crystals With Different Orientations

Transmittance (%)	Crystal Orientation	Pump Threshold (W)	Max. Output (W′)	Slope Efficiency(%)
5	X	0.76	7.07	53.6
	Y	0.43	9.43	51.3
	Z	0.53	8.43	55.9
10	X	1.14	6.86	53.3
	Y	0.55	9.30	51.3
	Z	0.55	8.34	55.9
40	X	4.41	3.05	32.6
	Y	2.69	5.35	33.3
	Z	2.67	5.29	39.3

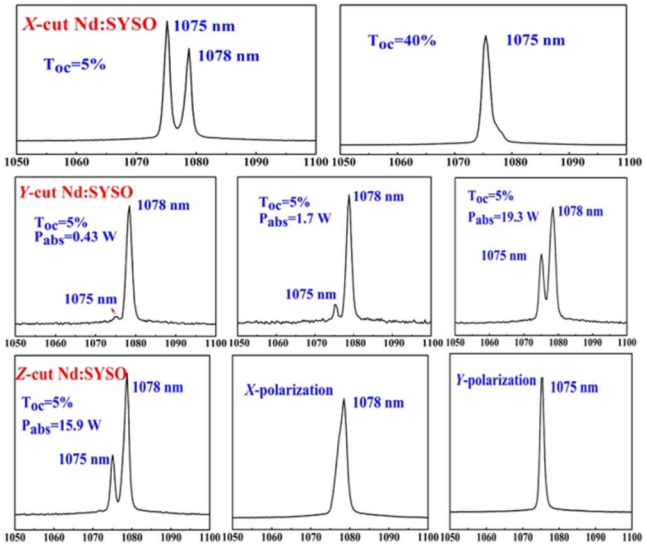

Fig. 6. Laser spectra of Nd:SYSO crystals obtained with different conditions.

measured the separated output power with the output coupler of $T_{oc} = 5\%$; the power for 1075 nm with Y polarization was 3.83 W, and that for 1078 nm with Z polarization was 0.54 W. So the individual component at 1075 or 1078 nm can be separated just by a simple beam splitter. With the output coupler of $T_{oc} = 40\%$, the X-cut Nd:SYSO laser was found to be single wavelength operation. It can be attributed to the smaller stimulated emission cross section at 1078 nm in the cases of both Y polarization and Z polarization and the larger transmittance loss. The spectra of the output lasers at different pump powers and output couplers were recorded in Fig. 6. For the Y-cut crystal, a maximum dual-wavelength average output power of 9.43 W was obtained, corresponding to an optical-to-optical conversion efficiency of 48.8%. With the output coupler of $T_{oc} = 5\%$, the X polarization and Z polarization laser powers were 6.48 and 0.76 W, respectively, under the absorbed pump power of 14 W. The X polarization laser component was found to be dual-wavelength simultaneous operation, with all three different output couplers. This phenomenon can also be explained by the contrast of the stimulated emission cross section; both at 1075 and 1078 nm, the stimulated emission cross sections of X polarization were larger than that of the Z polarization. For the Z-cut crystal, a maximum output power of 8.43 W was achieved, giving a slope conversion efficiency of 55.9%. As shown in Fig. 6, the Z-cut Nd:SYSO laser also operated at dual wavelength and that 1078 nm with X polarization and 1075 nm with Y polarization were found to have orthogonally polarized outputs.

This work was supported by the National Natural Science Foundation of China (No. 61505098), the Scientific Research Foundation of Shandong University of Science and Technology for Recruited Talents (No. 2015RCJJ013), the Postdoctoral Science Foundation of China (No. 2015M572062), the Qingdao City Innovative Leading Talent Plan (No. 13-CX-25), the CAEP THz Science and Technology Foundation (No. 201401), the Qingdao Economic & Technical Development Zone Science & Technology Project (No. 2013-1-64), and the SDUST Research Fund (Nos. 2012KYTD102 and 2015JQJH103).

References

1. Z. Yu, M. Wang, X. Hou, and W. Chen, Chin. Opt. Lett. **13**, 071403 (2015).
2. Y. J. Sun, C. K. Lee, J. L. Xu, Z. J. Zhu, Y. Q. Wang, S. F. Gaom, H. P. Xia, Z. Y. You, and C. Y. Tu, Photon. Res. **3**, A97 (2015).
3. F. Lou, R. W. Zhao, J. L. He, Z. T. Jia, X. C. Su, Z. W. Wang, J. Hou, and B. T. Zhang, Photon. Res. **3**, A25 (2015).
4. S. H. Wu, Z. S. Liu, and B. Y. Liu, J. Modern Opt. **53**, 333 (2006).
5. S. H. Rasta, A. Manivannan, and P. F. Sharp, Proc. SPIE **7368**, 736805 (2009).
6. P. Zhao, S. Ragam, Y. J. Ding, and I. B. Zotova, Opt. Lett. **35**, 3979 (2010).
7. X. Z. Wang, Z. F. Wang, Y. K. Bu, Z. Liu, L. J. Chen, G. X. Cai, Z. P. Cai, and J. M. Dawes, IEEE Photon. Technol Lett. **26**, 1983 (2014).
8. G. Shayeganrad, Y. C. Huang, and L. Mashhadi, Appl. Phys. B **108**, 67 (2012).
9. F. Pallas, E. Herault, J. F. Roux, A. Kevorkian, J. L. Coutaz, and G. Vitrant, Opt. Lett. **37**, 2817 (2012).
10. B. Wu, P. P. Jiang, D. Z. Yang, T. Chen, J. Kong, and Y. H. Shen, Opt. Express **17**, 6004 (2009).
11. A. Agnesi, S. Dell'Acqua, A. Guandalini, G. Reali, F. Cornacchia, A. Ton-celli, M. Tonelli, K. Shimamura, and T. Fukuda, IEEE J. Quantum Electron. **37**, 304 (2001).
12. K. Zhong, C. L. Sun, J. Q. Yao, D. G. Xu, X. Y. Xie, X. L. Cao, Q. L. Zhang, J. Q. Luo, D. L. Sun, and S. T. Yin, IEEE J. Quantum Electron. **49**, 375 (2013).
13. T. L. Feng, K. J. Yang, S. Z. Zhao, J. Zhao, W. C. Qiao, T. Li, L. H. Zheng, J. Xu, Q. G. Wang, X. D. Xu, L. B. Su, and Y. G. Wang, IEEE Photon. Technol. Lett. **27**, 7 (2015).
14. J. M. Serres, P. Loiko, X. Mateos, K. Yumashev, N. Kuleshov, V. Petrov, U. Griebner, M. Aguiló, and F. Díaz, Opt. Mater. Express **5**, 661 (2015).
15. P. A. Loiko, X. Mateos, N. V. Kuleshov, A. A. Pavlyuk, K. V. Yumashev, V. Petrov, U. Griebner, M. Aguiló, and F. Díaz, IEEE J. Quantum Electron. **50**, 669 (2014).
16. Y. G. Zhao, X. L. Li, M. M. Xu, H. H. Yu, Y. Z. Wu, Z. P. Wang, X. P. Hao, and X. G. Xu, Opt. Express **21**, 3516 (2013).
17. K. J. Yang, H. Bromberger, D. Heinecke, C. Kölbl, H. Schafer, T. Dekorsy, S. Z. Zhao, L. H. Zheng, J. Xu, and G. J. Zhao, Opt. Express **20**, 18630 (2012).
18. S. D. Liu, L. H. Zheng, J. L. He, J. Xu, X. D. Xu, L. B. Su, K. J. Yang, B. T. Zhang, R. H. Wang, and X. M. Liu, Opt. Express **20**, 22448 (2012).
19. J. Hou, L. H. Zheng, J. L. He, J. Xu, B. T. Zhang, Z. W. Wang, F. Lou, R. H. Wang, and X. M. Liu, Laser Phys. Lett. **11**, 035803 (2014).
20. Y. P. Huang, C. Y. Cho, Y. J. Huang, and Y. F. Chen, Opt. Express **20**, 5644 (2012).